International Journal of Nanomedicine

Dovepress
open access to scientific and medical research

Open Access Full Text Article

ORIGINAL RESEARCH

Electrospun silk fibroin/poly(lactide-co-ε-caprolactone) nanofibrous scaffolds for bone regeneration

This article was published in the following Dove Press journal:
International Journal of Nanomedicine
11 April 2016
Number of times this article has been viewed

Zi Wang[1,*]
Ming Lin[1,*]
Qing Xie[1]
Hao Sun[1]
Yazhuo Huang[1]
DanDan Zhang[1]
Zhang Yu[1]
Xiaoping Bi[1]
Junzhao Chen[1]
Jing Wang[2]
Wodong Shi[1]
Ping Gu[1]
Xianqun Fan[1]

[1]Department of Ophthalmology, Ninth People's Hospital, Shanghai Jiao Tong University School of Medicine, [2]Biomaterials and Tissue Engineering Laboratory, College of Chemistry & Chemical Engineering and Biotechnology, Donghua University, Shanghai, People's Republic of China

*These authors contributed equally to this work

Background: Tissue engineering has become a promising therapeutic approach for bone regeneration. Nanofibrous scaffolds have attracted great interest mainly due to their structural similarity to natural extracellular matrix (ECM). Poly(lactide-co-ε-caprolactone) (PLCL) has been successfully used in bone regeneration, but PLCL polymers are inert and lack natural cell recognition sites, and the surface of PLCL scaffold is hydrophobic. Silk fibroin (SF) is a kind of natural polymer with inherent bioactivity, and supports mesenchymal stem cell attachment, osteogenesis, and ECM deposition. Therefore, we fabricated hybrid nanofibrous scaffolds by adding different weight ratios of SF to PLCL in order to find a scaffold with improved properties for bone regeneration.

Methods: Hybrid nanofibrous scaffolds were fabricated by blending different weight ratios of SF with PLCL. Human adipose-derived stem cells (hADSCs) were seeded on SF/PLCL nanofibrous scaffolds of various ratios for a systematic evaluation of cell adhesion, proliferation, cytotoxicity, and osteogenic differentiation; the efficacy of the composite of hADSCs and scaffolds in repairing critical-sized calvarial defects in rats was investigated.

Results: The SF/PLCL (50/50) scaffold exhibited favorable tensile strength, surface roughness, and hydrophilicity, which facilitated cell adhesion and proliferation. Moreover, the SF/PLCL (50/50) scaffold promoted the osteogenic differentiation of hADSCs by elevating the expression levels of osteogenic marker genes such as *BSP*, *Ocn*, *Col1A1*, and *OPN* and enhanced ECM mineralization. In vivo assays showed that SF/PLCL (50/50) scaffold improved the repair of the critical-sized calvarial defect in rats, resulting in increased bone volume, higher trabecular number, enhanced bone mineral density, and increased new bone areas, compared with the pure PLCL scaffold.

Conclusion: The SF/PLCL (50/50) nanofibrous scaffold facilitated hADSC proliferation and osteogenic differentiation in vitro and further promoted new bone formation in vivo, suggesting that the SF/PLCL (50/50) nanofibrous scaffold holds great potential in bone tissue regeneration.

Keywords: human adipose-derived mesenchymal stem cells, silk fibrin, poly(lactide-co-ε-caprolactone), proliferation, osteogenesis

Correspondence: Ping Gu; Xianqun Fan
Department of Ophthalmology, Ninth People's Hospital, Shanghai Jiao Tong University School of Medicine, Zhizaoju Road NO. 639, Shanghai 200011, People's Republic of China
Tel +86 21 2327 1699*5587
Fax +86 21 6313 7148
Email guping2009@hotmail.com; fanxq@sh163.net

Introduction

Complex bone injuries and defects arising from trauma, tumor resection, and developmental deformities still present a difficult challenge for orthopedic surgeons worldwide in giving effective treatment. Autologous bone graft is the gold standard for clinical repair of bone defects.[1] However, autologous bone grafts are usually associated with drawbacks such as donor site morbidity, pain, second-site surgery, prolonged

submit your manuscript | www.dovepress.com
Dovepress
http://dx.doi.org/10.2147/IJN.S97445

hospitalization, and inadequate donor tissue availability.[2,3] An alternative option for treating bone defects is the use of an allogenic bone graft, which carries the risk of disease transmission and infection from donor to recipient.[4] Hence, bone tissue engineering involving the transplant of an appropriate scaffold alone or in combination with seed cells has become a promising therapeutic approach for bone regeneration.

Human adipose-derived stromal/stem cells (hADSCs) have received great attention in the field of tissue engineering, mainly due to their easy accessibility, abundant sources, rapid expansion, and capability of multiple lineage differentiation.[5] Also, adipose-derived stem cells (ADSCs) are reported to have the potential to readily undergo osteogenic differentiation independently of donor age and bone quality.[6–10] These characteristics make hADSCs an appealing seed cell for bone tissue engineering.

Nanofibrous scaffolds have attracted great interest in the tissue engineering field, mainly due to their structural similarity to the natural extracellular matrix (ECM).[11] Electrospinning is a convenient and inexpensive way to fabricate nanofibrous scaffolds. Generally, there are two groups of polymers capable of being electrospun, synthetic and natural. Synthetic polymers, including polycaprolactone (PCL), poly(L-lactic acid) (PLLA), poly(glycolic acid) (PGA), and their copolymers, are promising biomaterials in bone tissue engineering for supporting the osteogenic differentiation of stem cells.[12–17] Among these synthetic polymers, poly(lactide-co-ε-caprolactone) (PLCL), which is a copolymer of PLLA and PCL, has attracted research attention for its beneficial properties derived from both PCL and poly(lactide) such as a controllable degradation rate, high flexibility,[18,19] tunable elasticity, tensile strength,[20] and good biocompatibility.[21] Scaffolds made of PLCL have been successfully used in bone tissue engineering.[22,23] However, PLCL polymers are inert, lack natural cell recognition sites, and the surface of PLCL scaffold is hydrophobic, which presents limitations regarding biomaterial/cell interaction.[24,25] Hence, to make the biomaterial surfaces more conducive to cell attachment and spreading, natural polymers with inherent bioactivity are incorporated into PLCL which may result in modulation of the physicochemical properties of the PLCL scaffold.

Silk fibroin (SF) is a good candidate among natural polymers, mainly due to its excellent biocompatibility, minimal inflammatory response, good oxygen and water vapor permeability, and slow and controllable biodegradability.[26–28] In addition, SF supports mesenchymal stem cell (MSC) attachment, osteogenesis, and ECM deposition.[29] Furthermore, the SF-modified surface of the synthetic polymer poly(D,L-lactic acid) improves the interaction between osteoblasts and the scaffold.[30] Therefore, we fabricated hybrid nanofibrous scaffolds by adding different weight ratios of SF to PLCL. Systematic in vitro and in vivo experiments were conducted to evaluate the physiochemical properties of the SF/PLCL scaffolds, and explore the effects of SF/PLCL scaffolds on cell adhesion, viability, proliferation, and osteogenic differentiation and further test their ability to repair critical-sized calvarial defect (CSD). Based on these evaluations, we present a promising scaffold with good mechanical, physiochemical, and osteoinductive properties for bone regeneration.

Materials and methods

Materials

Bombyx mori silkworm cocoons were generously provided by Jiaxing Silk Co. Ltd. (Jiaxing, People's Republic of China). The PLCL polymer (with an average molecular weight of 300,000, poly(L-lactic acid) (LA) to polycaprolactone (CL) mole ratio 50:50) was supplied by Nara Medical University (Kashihara, Japan). The 1,1,1,3,3,3,-hexafluoro-2-propanol was purchased from Daikin (Daikin Industries Ltd., Osaka, Japan).

Preparation of SF/PLCL nanofibrous scaffold by electrospinning

Raw silk was degummed three times using a 0.5 wt% (0.02 M) Na_2CO_3 (Sigma-Aldrich Co., St Louis, MO, USA) solution at 100°C for 30 minutes each time to remove the sericin gum and washed with sterilized distilled water three times. Degummed silk was then dissolved in a ternary solvent system of $CaCl_2$/H_2O/ethanol (mole ratio 1/8/2) for 1 hour at 70°C. The SF solution was dialyzed through a cellulose tubular membrane (250–257 μm, Sigma) in distilled water for 3 days at room temperature (RT) and then filtered and lyophilized to obtain regenerated SF sponges. After PLCL and SF were dissolved in 1,1,1,3,3,3,-hexafluoro-2-propanol, different weight ratios of SF to PLCL (100:0, 75:25, 50:50, 25:75, 0:100) were blended to a final concentration of 8 w/v%, followed by magnetic stirring for 6 hours at RT. The solutions were placed in a 2.5 mL plastic syringe with a blunt-ended needle. The syringe was then placed in a syringe pump (789100C; Cole-Parmer Instrument Co., Vernon Hills, IL, USA) with a mass flow rate of 1 mL/h. The electrospinning used a high-voltage power supply (BGG6-358; BMEICO, Beijing, People's Republic of China) and a voltage of 12 kV was applied across the needle and ground collector. To collect the nanofibers, a flat steel plate covered with aluminum foil was placed in the opposite side of the needle, with a perpendicular distance of 11 cm from the needle. A steel rotating disk with a rotating speed of

1,500 rpm was used. The obtained material films were dried in vacuum (50 mbar, 25°C) for 72 hours.

Characterization of SF/PLCL nanofibrous scaffold

Scanning electron microscopy (SEM)

The electrospun nanofibrous scaffolds were cut into 8×8 mm pieces and coated with 10 nm of platinum before imaging by an SEM (JSM-6701; JEOL, Tokyo, Japan). The mean fiber diameters were estimated using image analysis software (Image-Pro Plus, Rockville, MD, USA) by selecting 60 fibers randomly from the SEM images.

Atomic force microscopy (AFM)

The roughness of the nanofibrous scaffold surfaces was measured using a scanning probe microscope (VECCO, New York, NY, USA) operated in AFM tapping mode at a microscopic level in air. The roughness value Ra represents the average distance between the surface and the mean line from recordings at each point and was calculated using the Nanoscope Image Processing software (VECCO).

Contact angle measurement

The contact angle was measured by a video contact angle instrument (Atension Theta, Turku, Finland), as previously reported,[21] to evaluate membrane surface wettability. A 0.8 µL droplet was dropped onto the scaffold, and the angles between the water droplet and the surface were measured at 15 seconds. Five samples were used for each test. The average value with standard deviation was reported.

Tensile strength tests

The tensile mechanical properties of the SF/PLCL scaffolds were measured using a tabletop MicroTester (Instron 5542; Instron, Norwood, MA, USA). Samples with different ratios of SF/PLCL were prepared with a thickness of 150–200 µm and cut into sizes of 10×20 mm. Stress–strain curves of each sample were recorded under the application of a static tensile load of 10 N capacity as previously reported.[31] Based on the stress–strain curves, the tensile strength and elongation at break were calculated. The highest stress prior to failure was the tensile strength of the sample. Five samples were tested for each group, and the mean data were collected.

Fourier transform infrared attenuated total reflectance spectroscopy (FTIR-ATR)

The FTIR-ATR spectra were obtained at RT in AVATAR 380 FTIR instrument (Thermo Fisher Scientific, Waltham, MA, USA) in the range 4,000–600 cm^{-1} at a resolution of 4 cm^{-1}.

X-ray diffractometer (XRD)

Wide-angle X-ray diffraction curves were obtained on an XRD (Riga Ku, Tokyo, Japan) within the scanning region of 2θ (5°–50°), with $Cu_{K\alpha}$ radiation (λ=1.5418 Å) at 40 kV and 40 mA.

Thermogravimetric analyzer (TGA)

The TGA experiments were performed using a NETZSCH STA 409C/3/F with a flow rate of 100 mL/min of nitrogen. Temperature was increased from RT to 1,000°C at a heating rate of 10°C/min.

Isolation and culture of human ADSCs

The hADSCs were isolated from human subcutaneous adipose tissue discarded from six outpatients who had undergone blepharoplasty (females, mean age 23.5 years, range 18–27 years), as previous reported.[32] The Medical Ethics Committee of Ninth People's Hospital, Shanghai Jiao Tong University School of Medicine approved the protocol in this study and written informed consents were obtained from all patients. In brief, adipose tissues were minced to small pieces and digested with 0.2% collagenase type 1 for 2 hours. The precipitated cells were cultured in α-MEM (Gibco BRL, Grand Island, NY, USA) containing 10% FBS and 100 units/mL penicillin at 37°C in an atmosphere of 5% CO_2. The medium was renewed three times a week.

Cell seeding

Before cell seeding, the nanofibrous scaffolds were sterilized with 75% ethanol vapor at 37°C for at least 24 hours and then placed under an ultraviolet lamp for 3 hours. These scaffolds were washed three times with sterilized phosphate-buffered saline (PBS) and soaked in complete culture medium at 37°C overnight. The hADSCs were seeded at a density of 1×10^4 cm^2 on electrospun nanofibrous scaffolds in 24-well plates.

Viability and morphology of hADSCs on SF/PLCL scaffold

Cell viability

The LIVE/DEAD Viability/Cytotoxicity Assay Kit (Invitrogen, Carlsbad, CA, USA) was used to distinguish viable cells from dead cells according to the protocol described by the manufacturer, as previously reported.[21] In brief, hADSCs cultured on the nanofibrous scaffolds or glass slips (control group) were incubated in PBS containing 2 mM

calcein acetoxymethyl ester and 2 mM ethidium homodimer 1 (Invitrogen) for 30 minutes at 37°C and then observed under a confocal laser scanning microscope (Carl Zeiss Microscopy, Oberkochen, Germany).

Cytotoxicity of SF/PLCL scaffolds

The cytotoxicity of the scaffolds of different blend ratios was assessed by measuring the cytosolic enzyme lactate dehydrogenase (LDH) released into the culture medium upon cell lysis using the CytoTox 96 Non-Radioactive Cytotoxicity Assay kit (Promega Biotech Co., Ltd., Beijing, People's Republic of China). Cytotoxicity (%) was expressed as the percentage of LDH released into the medium out of the total LDH activity.

Cell adhesion

Adhesion of hADSCs to the scaffolds was evaluated by counting the cells that adhered to the surface of the polymer at 4 and 24 hours after cell seeding. The hADSCs were cultured for 4 and 24 hours on different scaffolds, and at each time point, the adherent hADSCs were enzymatically (0.25% trypsin–0.1% ethylene diamine tetraacetic acid [EDTA]; Gibco) detached and counted using a hemocytometer. The cell adhesion rate was expressed as a percentage of the initial number of seeded cells.

Cell proliferation

Cell proliferation was examined using a cell counting kit-8 (CCK-8) according to the manufacturer's instructions (Dojindo Molecular Technologies, Inc., Tokyo, Japan), as previously reported.[34] For this purpose, 10 μL of CCK-8 solution was added to each well of the 96-well plate and incubated with the cells for 4 hours at 37°C. The absorbance was measured at a wavelength of 450 nm.

Scanning electron microscopy

The hADSCs were cultured on the nanofibrous scaffolds for 3 days, and the hADSCs seeded on the nanofibrous scaffolds underwent osteogenic differentiation for 14 days before being washed with PBS, fixed in 2% glutaraldehyde for 2 hours, dehydrated in a series of graded concentrations of ethanol, dried in vacuum, and gold-sputtered. The samples were imaged using SEM (JSM-6701; JEOL, Tokyo, Japan).

F-Actin observation

The hADSCs were cultured on the nanofibrous scaffolds for 3 days, and the cell-layered constructs were fixed with 4% paraformaldehyde (Sigma), then incubated for 30 minutes with 20 nM Alexa Fluor 488-conjugated phalloidin (Invitrogen). The cell nucleus was counterstained with 4',6-diamidino-2-phenylindole (DAPI) (Invitrogen) for 15 minutes at RT. Images were visualized and imaged on a Leica TCS SP8 microscope (Leica Microsystems, Wetzlar, Germany).

Analysis of in vitro osteogenic differentiation of hADSCs on SF/PLCL scaffolds

The hADSCs were seeded on the SF/PLCL scaffolds and maintained in standard culture conditions for 24 hours before being cultured in osteogenic induction medium (complete medium supplemented with 50 μg/mL ascorbic acid, 0.01 M glycerol-2-phosphate, and 10^{-7} M dexamethasone, all from Sigma).

Alkaline phosphatase (ALP) activity

The hADSCs were seeded on the different scaffolds at a density of 1.0×10^5 cells/well and cultured in osteogenic induction medium. At day 7, ALP staining was performed using a 5-bromo-4-chloro-3-indolyl phosphate/nitroblue tetrazoli (BCIP/NBT) Alkaline Phosphatase Color Development Kit (Beyotime Institute of Biotechnology, Shanghai, People's Republic of China) according to the manufacturer's instructions.[35] Semiquantitative analysis of ALP activity was performed as previously reported.[36] In brief, the cells were lysed using radio immunoprecipitation assay (RIPA) lysis buffer (Beyotime Institute of Biotechnology) and the total concentration of protein content was determined using a bicinchoninic acid (BCA) protein assay kit. Using *p*-nitrophenyl phosphate (Sigma) as the substrate, ALP activity was measured from the absorbance at 405 nm. The ALP levels were normalized to the total protein content.

Mineralization of ECM detection

The calcium deposition and mineralization of osteoblastic ECM were detected by alizarin red S (ARS) staining and SEM. At day 14, the cells were fixed in 2% glutaraldehyde and examined by SEM. The cells on all types of scaffolds were also fixed and stained with ARS (1%, pH=4.1, Sigma) for 30 minutes at 37°C. For the semiquantitative analysis of ARS, the stain was desorbed with 10% cetylpyridinium chloride (Sigma) for 1 hour. The solution was collected and distributed at 100 μL per well on a 96-well plate for absorbance reading at 590 nm using a spectrophotometer (Thermo Spectronic, Carlsbad, CA, USA). The ARS levels were normalized to the total protein content.

Immunocytochemistry

The hADSCs were seeded on nanofibrous scaffolds in 24-well plates and cultured in osteogenic induction

medium for 14 days. The cells were then fixed with 4% paraformaldehyd (PFA) (Sigma) and incubated in blocking buffer for 1 hour at RT, as reported.[37] The cells were incubated with *BSP* and SATB2 (1:200; Abcam, Cambridge, MA, USA) overnight at 4°C and then incubated with fluorescently labeled secondary antibodies (1:800, Alexa Fluor546-goat anti-rabbit/mouse; BD Biosciences, San Jose, CA, USA) for 1 hour at RT. The cell nucleus was counterstained with DAPI (Invitrogen) for 15 minutes at RT. Immunoreactive cells were visualized and imaged on a Leica TCS SP8 microscope (Leica Microsystems). Images were constructed using Leica LAS AF software (Leica Microsystems, Heidelberg, Germany).

Total RNA isolation and reverse transcription and quantitative polymerase chain reaction (qPCR)

RNA isolation and qPCR were performed as previously reported.[25] Scaffolds with cells were immersed into RNA extract buffer and ground on ice using a Bio-gen pro200 Homogenizer (PRO Scientific Inc., Oxford, UK). An RNeasy Mini Kit (Qiagen, Valencia, CA, USA) was used to extract total RNA. Then, 2 μg of total RNA was reverse transcribed in a 20 μL reaction volume using the PrimeScript™ RT Reagent Kit (Perfect Real Time; TaKaRa Biotechnology [Dalian] Co., Ltd., Dalian, People's Republic of China) according to the protocol described by the manufacturer. The qPCR was conducted in a 20 μL reaction volume containing 10 μL of reaction mixture, 1 μL of complementary DNA, and 2 μL of primers using the Power SYBR Green PCR Master Mix (Thermo Fisher Scientific, Waltham, MA, USA) and a 7,500 Real-Time PCR Detection System. The primers are shown in Table 1. Each target gene was tested in triplicate. The relative gene expressions were expressed as the fold change relative to the untreated controls after normalization to the expression of glyceraldehyde-3-phosphatedehydrogenase (GAPDH).

Western blot analysis

The procedure was performed according to standard protocols. In brief, cells were lysed with RIPA lysis buffer (Beyotime Institute of Biotechnology, Shanghai, People's republic of China), supplemented with 1 nM phenylmethanesulfonyl fluoride (PMSF) (Invitrogen), then the collected protein contents were determined using a BCA protein assay kit (Thermo Fisher Scientific). Equal amounts of cell lysates were loaded in 10% sodium dodecyl sulfate-polyacrylamide gel electrophoresis gel and transferred to a polyvinylidene fluoride membrane (0.22 μm; EMD Millipore, Billerica, MA, USA). After blocking with 5% nonfat milk, the membranes were incubated with primary antibodies: anti-*BSP* (1:1,000, Abcam), anti-*OPN* (1:1,000, Abcam), anti-*Ocn* (1:1,000, Abcam), and anti-β-actin (1:3,000, Abcam) at 4°C overnight and then incubated for 1 hour with fluorescein-conjugated secondary antibodies (Abcam) at RT. Protein expression images were visualized using Odyssey V 3.0 image scanning (LI-COR Biosciences, Lincoln, NE, USA). Relative protein levels were normalized against β-actin. All experiments were performed in triplicate.

Animal experiments

All procedures were approved by the Animal Research Committee of Ninth People's Hospital, Shanghai Jiao Tong University School of Medicine. Surgical procedures were performed on Sprague Dawley rats (8 weeks old, female, weight: 150–180 g), as previously reported.[38] All animals received an oral dose of 100 mg/mL cyclosporine beginning 4 days prior to transplantation and continued until the last day of the experiment, according to a previous study.[33] In brief, the animals were generally anesthetized (Nembutal 3.5 mg/100 g). The cranium was exposed by a blunt incision made on the scalp. A critical-sized cranial defect was made using an 8 mm-diameter trephine (Nouvag AG, Goldach, Switzerland), and a composite of nanofibrous scaffold and hADSCs was used to repair the CSDs of the rats. Eighteen rats were randomly allocated into the following graft study groups: 1) hADSCs/SF/PLCL (50/50), 2) hADSCs/pure PLCL, and 3) control (empty PLCL scaffold). The cell-seeded scaffolds were implanted into the defects, and the incisions were closed in layers using 4–0 resorbable sutures.

Table 1 Primers used for qPCR

Genes	Accession no	Forward (5′–3′)	Reverse (5′–3′)
BSP	NM_004967	cactggagccaatgcagaaga	tggtggggttgtaggttcaaa
OPN	NM_001251830	ctccattgactcgaacgactc	caggtctgcgaaacttcttagat
Ocn	NM_199173	cactcctcgccctattggc	ccctcctgcttggacacaaag
Col1A1	NM_000088.3	gtttggcctgaagcagagac	tctaaatgggccacttccac
GAPDH	NM_001256799	ggagcgagatccctccaaaat	ggctgttgtcatacttctcatgg

Abbreviation: qPCR, quantitative polymerase chain reaction.

Microcomputed tomography (micro-CT) measurement

At 8 weeks post-operation, the specimens were collected and evaluated using an animal micro-CT scanner (mCT-80; Scanco Medical, Zurich, Switzerland) in high-resolution scanning mode (pixel matrix, 1,024; voxel size, 20 mm; slice thickness, 20 mm), as previously reported.[39] Data were analyzed using the micro-CT image analysis software (Scanco Medica), including the bone mineral density and the percentage of new bone volume relative to tissue volume (BV/TV).

Sequential fluorescent labeling

Polychrome sequential fluorescent labeling for new bone formation was performed as described previously.[38] The animals were intraperitoneally injected with fluorochromes as follows: tetracycline (1 mg/kg of body weight), alizarin red (3% in 2% sodium bicarbonate solution, 0.8 mL/kg of body weight), and calcein (1% in 2% sodium bicarbonate solution, 5 mL/kg of body weight) (all from Sigma) at 3, 6, and 9 weeks after the operation.

Histological and histomorphometric analysis

The skulls were harvested 12 weeks post-implantation. After dehydration in ascending concentrations of alcohol from 75% to 100%, the samples were embedded in polymethylmethacrylate. Three sagittal sections of the central area were cut and polished to a final thickness of ~40 mm as previously reported.[40] The sections were stained with van Gieson's picrofuchsin. Areas of newly formed bone were quantified using Image Pro Plus™ (Media Cybernetics, Silver Springs, MD, USA) and reported as a percentage of the entire bone defect area.

Statistical analysis

All quantitative data are presented as the mean ± standard deviation unless specifically indicated otherwise. Each experiment was repeated at least three times. Statistical significance was determined using the unpaired Student's *t*-test, and a value of $P<0.05$ was considered to be statistically significant.

Results

Characterization of SF/PLCL nanofibrous scaffolds

The scanning electron micrographs of the SF/PLCL electrospun nanofibrous scaffolds showed that the scaffolds consisted of randomly distributed fibers (Figure 1A) and the average fiber diameter ranged from 166.6 to 536 nm with increasing PLCL content (Table 2). Figure 1B shows the results of AFM of different weight ratios of SF/PLCL electrospun scaffolds. The surface roughness of pure SF and pure PLCL, shown as Ra, was lower than for the blended SF/PLCL scaffolds, suggesting that blending SF with PLCL resulted in an increase in surface roughness. The Ra of the SF/PLCL (50/50) scaffold was 265 nm, which was the highest among the five scaffolds. Then, in wettability analysis, representative images of the water contact angles of SF/PLCL electrospun nanofibrous scaffolds at 15 seconds showed that pure SF was highly hydrophilic and pure PLCL was hydrophobic (Figure 1C). The water contact angles were 37.18°±1.65°, 46.6°±1.4°, 62.02°±1.31°, 97.93°±2.20°, and 116.44°±2.74° for the pure SF, SF/PLCL (75/25), SF/PLCL (50/50), SF/PLCL (25/75), and pure PLCL scaffolds, respectively (Figure 1D). As shown in Figure 1E, the tensile strength of the SF/PLCL electrospun nanofibrous scaffolds gradually increased with increasing PLCL concentrations. Furthermore, FTIR-ATR spectra of nanofibrous scaffolds are shown in Figure S1A. The characteristic absorption band at 3,327 cm^{-1} is attributed to –N–H and the characteristic absorption bands at 1,617 and 1,532 cm^{-1} are ascribed to C=O stretching (amide I) and N–H bending (amide II), respectively, and these bands only existed in the scaffolds composed of SF. The characteristic absorption band at 1,746 cm^{-1} is attributed to O–C=O; this absorption band existed only in the scaffolds composed of PLCL and the peak of this band increased in these scaffolds along with the increase in the concentration of PLCL. In addition, XRD curves of these five electrospun fibrous scaffolds are shown in Figure S1B. XRD analysis of SF showed broad peak at 2θ (21.1°). PLCL fibrous scaffolds exhibited crystalline diffraction peaks at 2θ (16.8°, 19.1°), respectively. The blended SF/PLCL scaffolds had both the broad peak and crystalline diffraction peaks, and the crystalline diffraction peaks became more obvious in these scaffolds along with the increase in the concentration of PLCL in the scaffold. Additionally, TGA curves showed that there were no differences in the shapes of the graphs among the five scaffolds (Figure S1C). All scaffolds first showed a rapid weight loss due to dehydration, followed by a period of steady gradual weight loss. A substantial weight loss followed the gradual decrease in weight as heating temperature increased. Differences in temperature in which the scaffold commenced rapid decomposition were observed in the five scaffolds. PLCL commenced decomposition at higher temperatures than SF, and this temperature in SF/PLCL-blended scaffolds increased

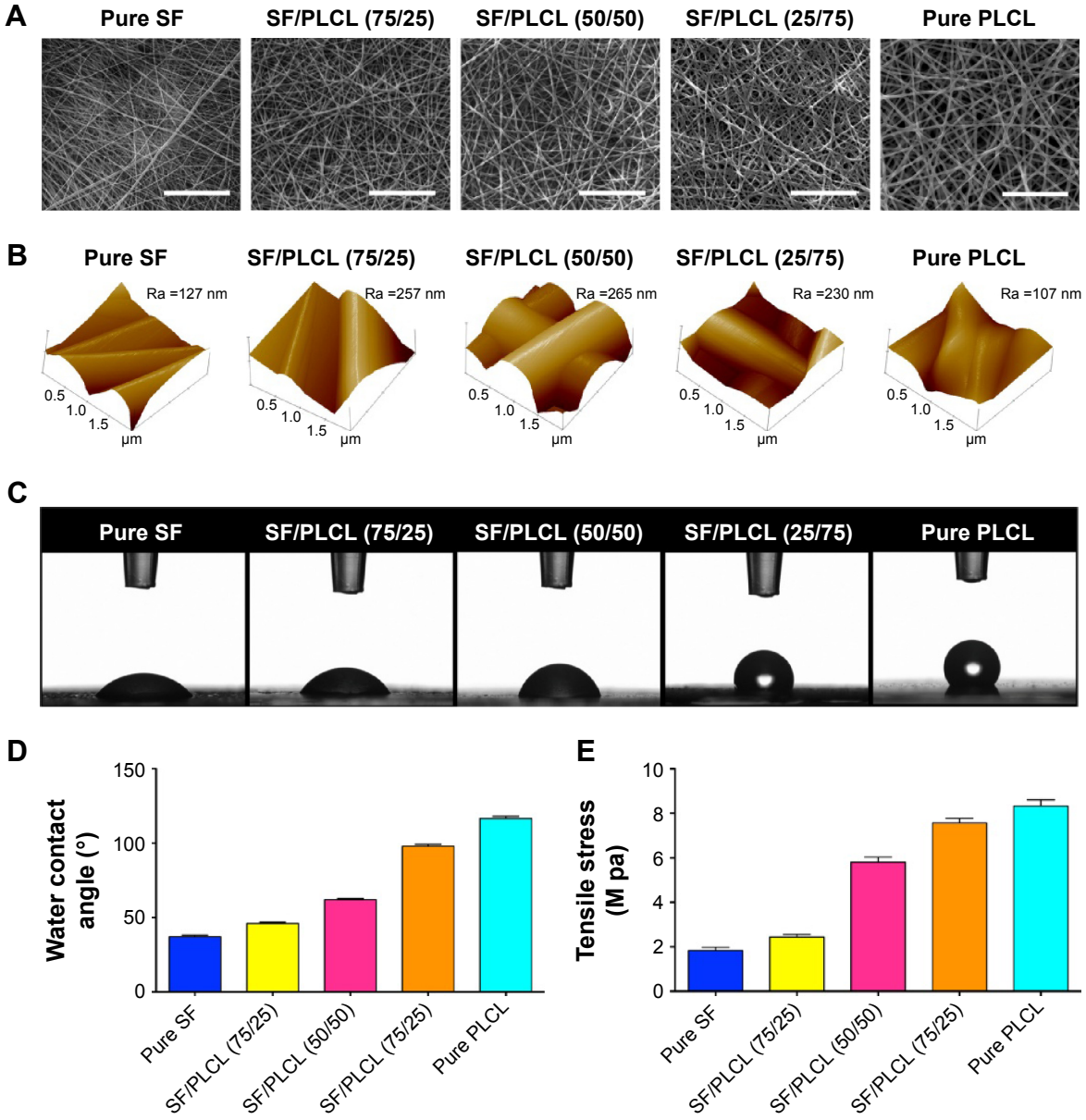

Figure 1 Characterization of SF/PLCL nanofibrous scaffolds of different weight ratios.
Notes: (**A**) Representative scanning electron microscopy images of SF/PLCL nanofibrous scaffolds of different weight ratios: pure SF, SF/PLCL (75/25), SF/PLCL (50/50), SF/PLCL (25/75), and pure PLCL. Scale bars: 20 μm. (**B**) Atomic force microscopy images of SF/PLCL nanofibrous scaffolds of different weight ratios. The roughness value Ra represents the average distance between the surface and the mean line from the recordings at each point. The roughness value Ra represents the average distance between the surface and the mean line from recordings at each point. (**C**) Representative images of water contact angle of SF/PLCL nanofibrous scaffolds of different weight ratios at 15 seconds. (**D**) Water contact angle of SF/PLCL nanofibrous scaffolds of different weight ratios. (**E**) Tensile strength of SF/PLCL nanofibrous scaffolds of different weight ratios.
Abbreviations: PLCL, poly(lactide-co-ε-caprolactone); SF, silk fibroin.

along with the increase in PLCL content in the scaffold. Rapid weight loss commenced at 283°C and 341°C for pure SF and pure PLCL, respectively. Above all, the hybrid SF/PLCL nanofibrous scaffolds exhibited increased surface roughness and improved hydrophilicity, compared with the pure PLCL scaffold; the SF/PLCL (50/50) scaffold exhibited the highest surface roughness and favorable hydrophilicity among the five scaffolds. The blending of SF and PLCL made the hybrid SF/PLCL scaffolds possess characteristics of both materials, and all scaffolds were thermally stable.

Adhesion, viability, and proliferation of hADSCs on SF/PLCL nanofibrous scaffolds

The hADSCs are regarded as a promising seed cell type in bone tissue engineering, and we investigated the

Table 2 The average fiber diameter of the SF/PLCL nanofibrous scaffold

Sample	Diameter (mean ± SD nm)
Pure SF	166.6±29.95
SF/PLCL (75/25)	241.6±41.24
SF/PLCL (50/50)	252.2±33.15
SF/PLCL (25/75)	319.8±75.75
Pure PLCL	536.1±95.46

Abbreviations: PLCL, poly(lactide-co-ε-caprolactone); SD, standard deviation; SF, silk fibroin.

biocompatibility of hADSCs and SF/PLCL nanofibrous scaffolds in this study. First, a Live/Dead staining analysis showed that only a few dead cells, which were stained red, could be seen in all cultures grown on the scaffolds (Figure 2A), indicating that the different weight ratios of the SF/PLCL electrospun scaffolds were all safe for the growth of hADSCs. Second, the adhesion of hADSCs on different scaffolds was assessed at 4 and 24 hours post-seeding. The adhesion rate of hADSCs seeded onto the SF/PLCL (50/50) scaffold was significantly higher than on the other scaffolds at both time points (Figure 2B). Then, to determine the effect of different scaffolds on supporting cell growth, we seeded hADSCs on different scaffolds and measured cell proliferation ability by the CCK-8 assay. The CCK-8 results demonstrated that the scaffold with 50/50 weight ratio was the most suitable of the tested scaffolds for hADSC proliferation (Figure 2C). In addition, to evaluate the toxicity of the scaffolds, the cytosolic enzyme LDH released into the

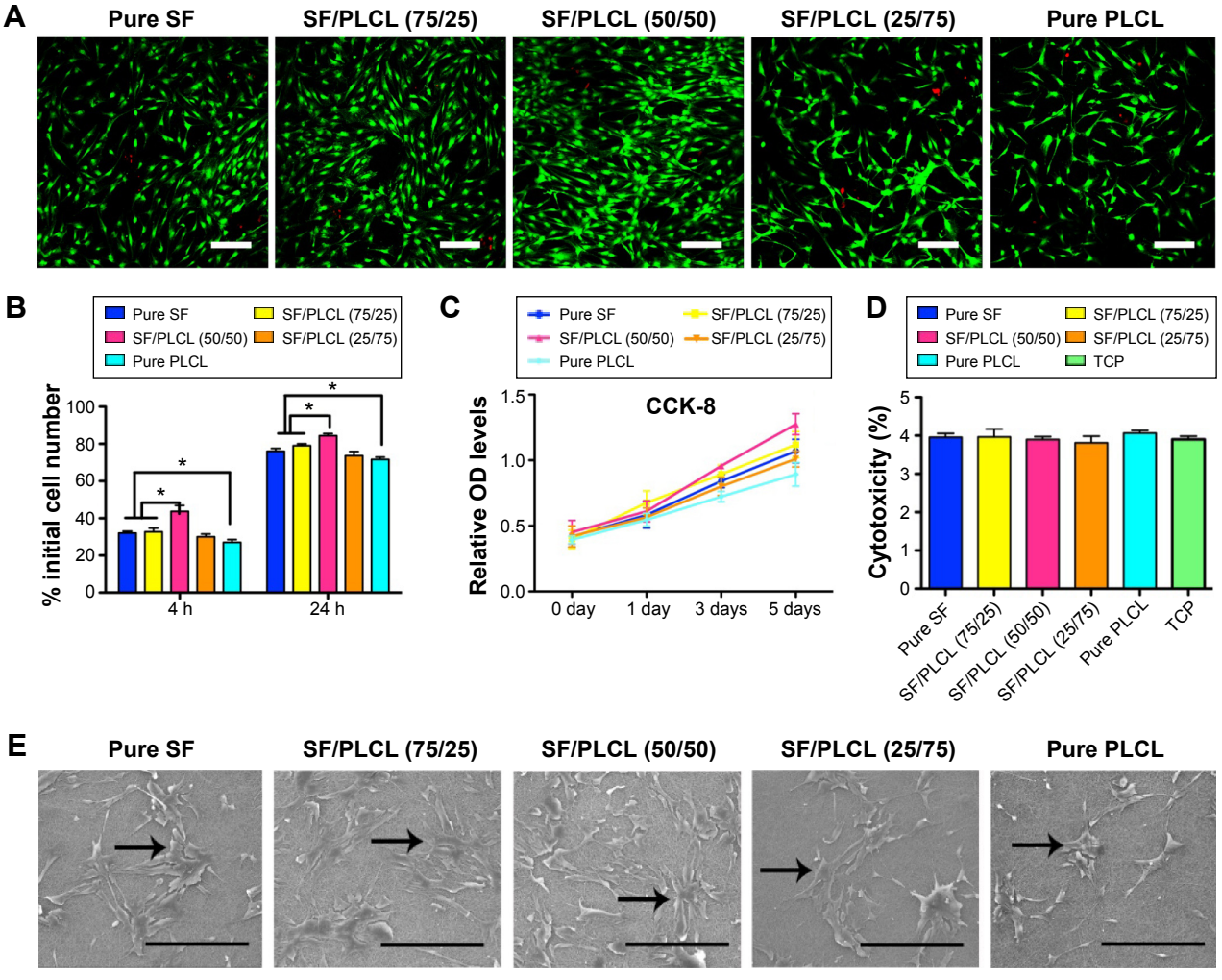

Figure 2 Adhesion, viability, and proliferation of hADSCs on SF/PLCL nanofibrous scaffolds of different weight ratios.
Notes: (**A**) Live/Dead staining of hADSCs on SF/PLCL nanofibrous scaffolds of different weight ratios after 3 days of culture. Scale bars: 200 μm. (**B**) Cell adhesion rates 4 and 24 hours post-cell seeding on SF/PLCL nanofibrous scaffolds of different weight ratios (*$P<0.05$). (**C**) CCK-8 analysis of the proliferation of hADSCs on SF/PLCL nanofibrous scaffolds of different weight ratios showed that the hADSCs on the SF/PLCL (50/50) scaffolds proliferated much more quickly than on other scaffolds. (**D**) LDH assays for acute cytotoxicity analysis of SF/PLCL nanofibrous scaffolds of different weight ratios showed no significant difference among groups. (**E**) Representative scanning electron microscopy images of hADSCs seeded on SF/PLCL nanofibrous scaffolds of different weight ratios after 3 days of culture. Scale bars: 300 μm.
Abbreviations: TCP, tissue culture plate; CCK-8, cell counting kit-8; hADSCs, human adipose-derived stem cells; LDH, lactate dehydrogenase; PLCL, poly(lactide-co-ε-caprolactone); SF, silk fibroin; h, hours.

culture medium was examined. No significant difference in LDH levels was observed among the cells grown on different SF/PLCL scaffolds (Figure 2D), suggesting that all of the scaffolds were nontoxic to the cultured cells. Furthermore, to visualize the morphology of the hADSCs seeded on different SF/PLCL scaffolds, SEM images depicting cell adhesion and morphology were taken at day 3 after cell seeding on the scaffolds. The hADSCs spread on all electrospun SF/PLCL scaffolds, exhibiting polygonal shapes and random orientations (Figure 2E). Additionally, the fluorescence images of hADSCs seeded on different scaffolds with cytoskeletons in green and nuclei in blue showed that cells on pure SF, SF/PLCL (75/25), and SF/PLCL (50/50) exhibited more actin stress fibers than those on SF/PLCL (25/75) and pure PLCL scaffolds (Figure S2). In addition, the number of cells grown on the pure SF, SF/PLCL (75/25), and SF/PLCL (50/50) scaffolds was higher than the number of cells grown on the pure PLCL scaffold, and the highest cell number was observed on the SF/PLCL (50/50) scaffold (Figure 2E), which was consistent with the results of the Live/Dead staining (Figure 2A).

Taken together, our results suggest that the SF/PLCL (50/50) scaffold was nontoxic and supported better proliferation of hADSCs than the scaffolds of other ratios.

Osteogenic differentiation of hADSCs on SF/PLCL nanofibrous scaffolds

ALP activity can be considered a biomarker for bone formation. In this study, the ALP staining (Figure 3A) and the semiquantification analysis (Figure 3B) showed that hADSCs

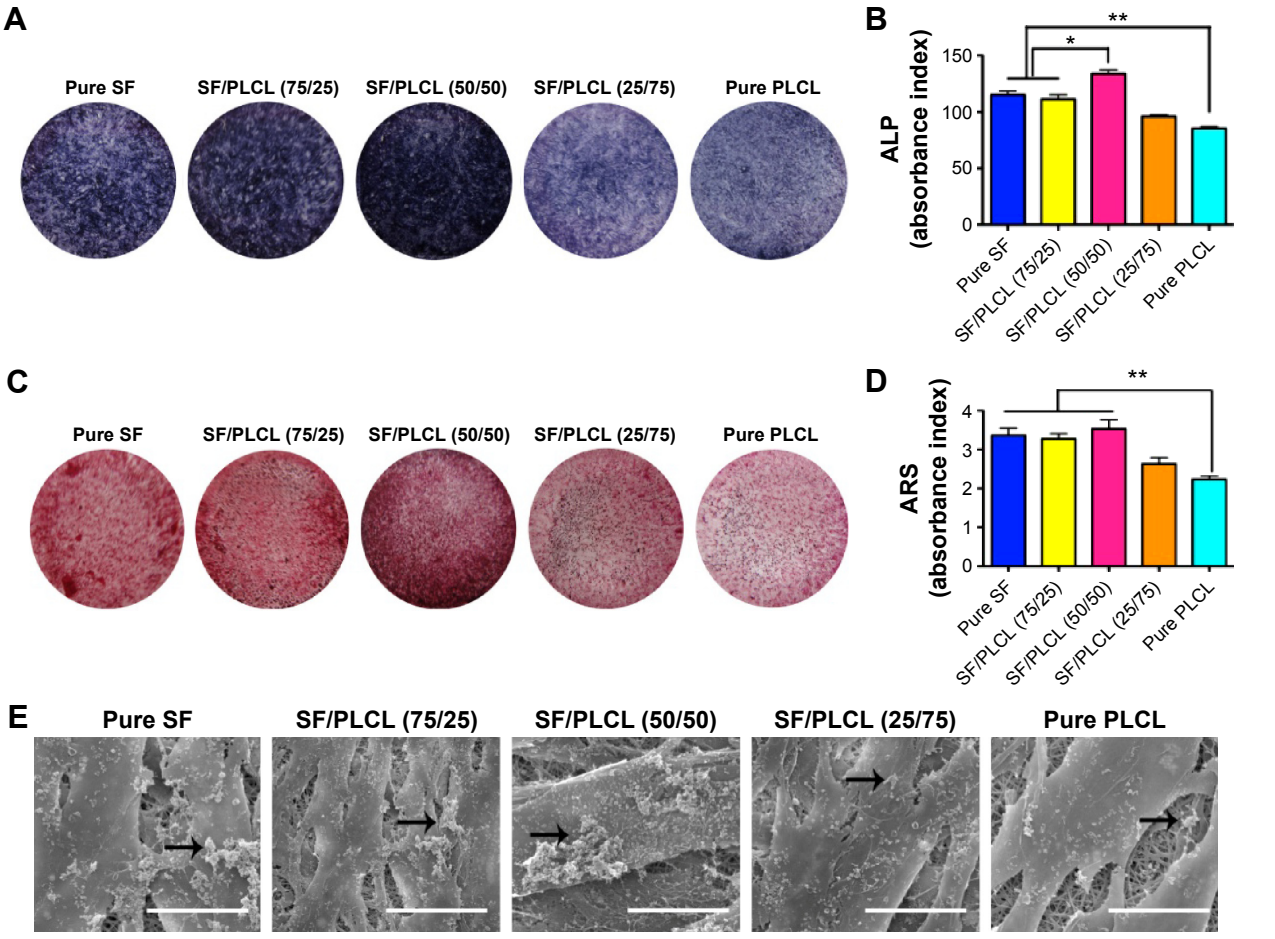

Figure 3 ALP activity and biomineralization of hADSCs on SF/PLCL nanofibrous scaffolds of different weight ratios.

Notes: (**A**) ALP staining of hADSCs on SF/PLCL nanofibrous scaffolds of different weight ratios after 7 days of osteogenic induction. (**B**) Semiquantitative analysis of ALP activity showed that the intracellular ALP level of the hADSCs was significantly higher on the SF/PLCL (50/50) scaffold than on other scaffolds (*$P<0.05$, **$P<0.01$). (**C**) ARS staining of hADSCs on SF/PLCL nanofibrous scaffolds of different weight ratios after 14 days of osteogenic induction. (**D**) Semiquantitative analysis of ARS staining showed that the mineralization of hADSCs on scaffolds of pure SF, SF/PLCL (75/25), and SF/PLCL (50/50) were markedly higher than on scaffolds of pure PLCL (**$P<0.01$). (**E**) Representative scanning electron microscope images of the biomineralization of hADSCs on electrospun SF/PLCL scaffolds of different weight ratios after 14 days of osteogenic induction. The deposition of crystallized particles (arrows point to examples) was clearly higher on the surfaces of the hADSCs on the pure SF, SF/PLCL (75/25), and SF/PLCL (50/50) scaffolds than on other scaffolds. Scale bars: 20 μm.

Abbreviations: ALP, alkaline phosphatase; ARS, alizarin red S; hADSCs, human adipose-derived stem cells; PLCL, poly(lactide-co-ε-caprolactone); SF, silk fibroin.

seeded on the SF/PLCL (50/50) scaffold exhibited significantly higher ALP activity than on scaffolds with other ratios after 7 days of culture in osteogenic medium. In addition, we evaluated the matrix mineralization by ARS assays of hADSCs seeded on different scaffolds after osteogenic induction for 14 days. As shown in Figure 3C, calcium deposition was higher in the pure SF, SF/PLCL (75/25), and SF/PLCL (50/50) groups than in the SF/PLCL (25/75) and pure PLCL groups, and the results from the quantification of extracted ARS (Figure 3D) were consistent with the results of ARS staining. Furthermore, the SEM images of the mineralization of hADSCs cultured on the different scaffolds demonstrated that the deposition of crystallized particles was more obvious on the surfaces of the pure SF, SF/PLCL (75/25), and SF/PLCL (50/50) scaffolds and that these depositions were qualitatively greater on the SF/PLCL (50/50) scaffold (Figure 3E). Additionally, after incubation in osteogenic medium for 14 days, the expression levels of osteogenic-specific genes of hADSCs on different electrospun SF/PLCL scaffolds were detected by qPCR, as shown in Figure 4A. The mRNA expression levels of *BSP*, *Ocn*, Col1A, and *OPN* were notably upregulated in the SF/PLCL (50/50) group compared with other groups. Moreover, fluorescent images of the distribution of *BSP* and transcriptional factor SATB2 expression of hADSCs are shown in Figure 4B. The percentage of *BSP*-positive cells was significantly higher on the SF/PLCL (50/50) scaffold than on other scaffolds (Figure 4C), and the ratio of SATB2-positive cells cultured on the SF/PLCL (50/50) scaffold was markedly upregulated compared with that of cells cultured on other scaffolds (Figure 4D). As observed in Figure 4E and F, the western blot analysis showed that the protein expression levels of *OPN*, *BSP*, and *Ocn* of the cells seeded on the pure SF, SF/PLCL (75/25), and SF/PLCL (50/50) scaffolds were significantly higher than the protein expression levels of the cells seeded on the pure PLCL scaffold.

Collectively, these results showed that blended SF/PLCL scaffolds enhanced hADSC osteogenic differentiation in vitro and that the SF/PLCL (50/50) scaffold performed the best.

In vivo osteogenesis

To evaluate the in vivo bone formation of the combination of hADSCs and nanofibrous scaffold, hADSCs seeded on nanofibrous scaffolds were used to repair CSDs in rats. The SF/PLCL (50/50) scaffold was chosen for the in vivo analyses due to its performance in the in vitro examinations, and the PLCL scaffold was used as positive control. To observe new bone formation within the defects, the morphology of the newly formed bone was measured using micro-CT at week 12 post-implantation. Representative images of each group are shown in Figure 5A, and new bone formation was observed in all groups. New bone formation in the SF/PLCL (50/50) group was greater than in the pure PLCL group and the control group (empty PLCL scaffold). In addition, a quantitative morphometric analysis using the micro-CT analysis system demonstrated that the BV/TV ratio in the SF/PLCL (50/50) group (56.42%±5.65%) was notably higher than in the pure PLCL and control groups (43.3%±6.24% and 10.59%±1.12%, respectively) ($P<0.05$) (Figure 5B). The trabecular number showed the same pattern as the BV/TV ratio (Figure 5C). Furthermore, the bone mineral density was much higher in the SF/PLCL (50/50) group (0.01676±0.00114 g/cc) than in the pure PLCL group (0.013360±0.00129 g/cc) and the control group (0.001578±0.000931 g/cc) ($P<0.05$) (Figure 5D). Taken together, these results indicated that the SF/PLCL (50/50) scaffold promoted bone regeneration much more prominently than the pure PLCL scaffold.

New bone formation was further investigated by tetracycline, alizarin red, and calcein fluorescence quantification analysis, representing the mineralization levels at different time points (Figure 6A). The percentage of tetracycline labeling (yellow) was 7.29%±0.87% for the SF/PLCL (50/50) group, which was greater than the percentages in the pure PLCL group (4.71%±1.17%) and the control group (1.02%±0.42%) ($P<0.05$). The percentages of calcein labeling (green) were 7.14%±0.98%, 3.56%±1.09%, and 1.17%±0.29% for the SF/PLCL (50/50), pure SF, and control groups, respectively ($P<0.05$), displaying significant differences between the SF/PLCL (50/50) and the pure PLCL and control groups ($P<0.05$). In addition, the percentage of alizarin red labeling (red) showed a similar tendency to tetracycline and the calcein labeling (Figure 6B). Taken together, these data suggest that the SF/PLCL (50/50) scaffold enhanced new bone formation.

The histological results obtained from the van Gieson staining of nondecalcified specimens (Figure 7A) were consistent with the micro-CT findings, as shown in Figure 5. The results from light microscopy demonstrated that the percentage of new bone area after 12 weeks was 32.66%±7.12% in the SF/PLCL (50/50) group, 24.48%±4.78% in the pure PLCL group, and 8.37%±2.65% in the control group (Figure 7B). As shown in Figure 7C, the areas of newly formed bone in the SF/PLCL (50/50) group (0.16313±0.045 cm^2), pure PLCL group (0.10531±0.029 cm^2), and control group (0.05598±0.026 cm^2) were calculated using light microscopy. These data indicated that the SF/PLCL (50/50) scaffold could

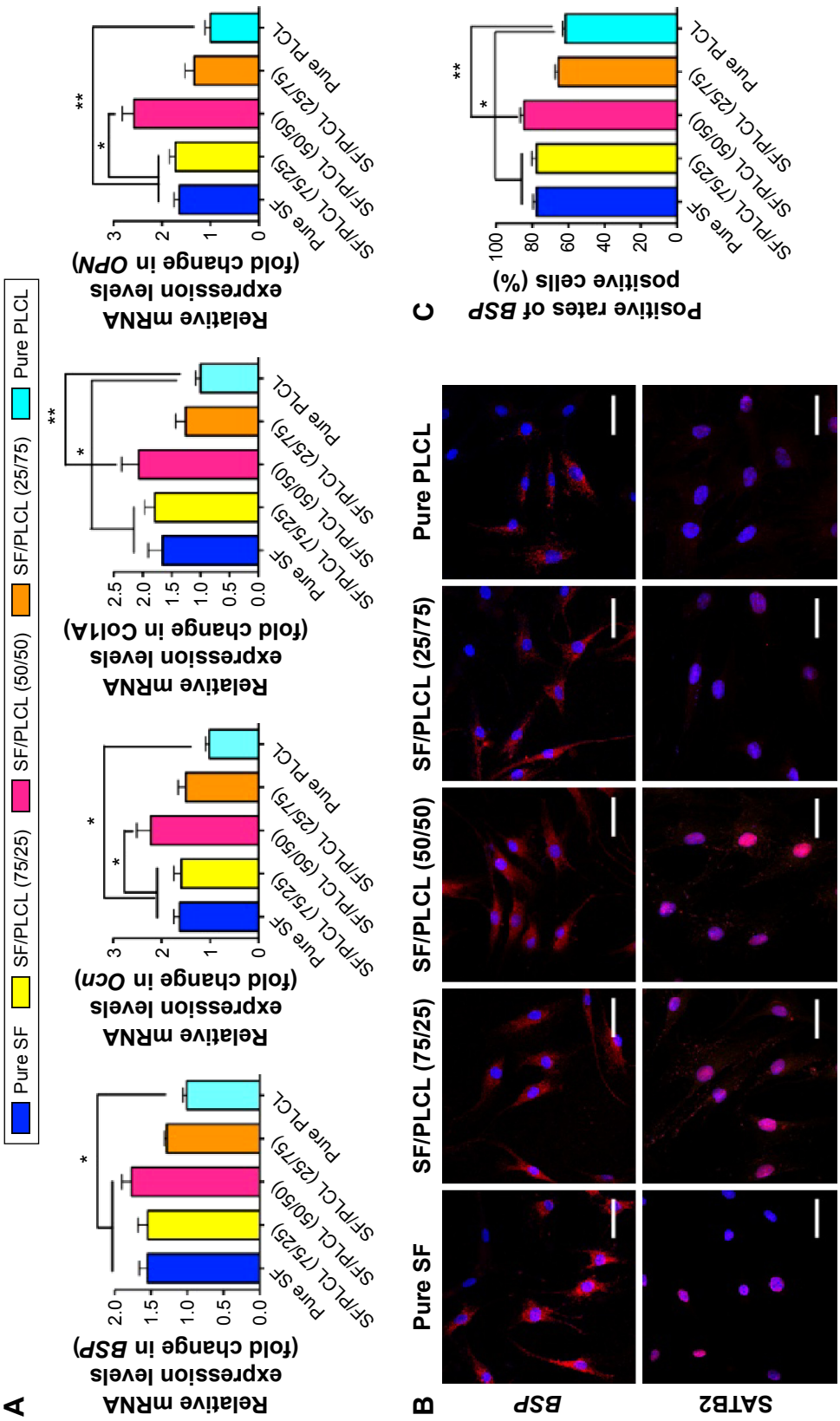

Figure 4 (*Continued*)

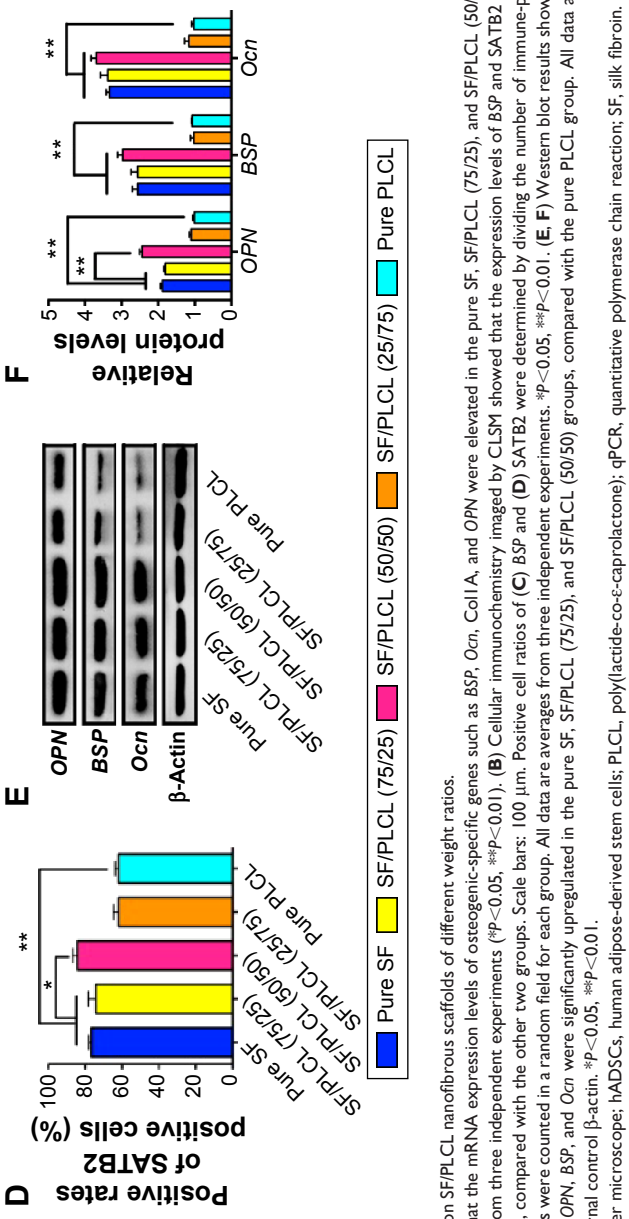

Figure 4 Osteogenesis of hADSCs on SF/PLCL nanofibrous scaffolds of different weight ratios.

Notes: **(A)** qPCR results showed that the mRNA expression levels of osteogenic-specific genes such as *BSP*, *Ocn*, Col I A, and *OPN* were elevated in the pure SF, SF/PLCL (75/25), and SF/PLCL (50/50) groups, compared with the pure PLCL group. All data are averages from three independent experiments (*$P<0.05$, **$P<0.01$). **(B)** Cellular immunochemistry imaged by CLSM showed that the expression levels of *BSP* and SATB2 were higher in the pure SF, SF/PLCL (75/25), and SF/PLCL (50/50) groups, compared with the other two groups. Scale bars: 100 μm. Positive cell ratios of **(C)** *BSP* and **(D)** SATB2 were determined by dividing the number of immune-positive cells by the number of nuclei stained with Hoechst; 700–1,000 cells were counted in a random field for each group. All data are averages from three independent experiments. *$P<0.05$, **$P<0.01$. **(E, F)** Western blot results showed that the protein expression levels of osteogenic-specific genes such as *OPN*, *BSP*, and *Ocn* were significantly upregulated in the pure SF, SF/PLCL (75/25), and SF/PLCL (50/50) groups, compared with the pure PLCL group. All data are averages from three independent experiments, normalized to the internal control β-actin. *$P<0.05$, **$P<0.01$.

Abbreviations: CLSM, confocal laser microscope; hADSCs, human adipose-derived stem cells; PLCL, poly(lactide-co-ε-caprolactone); qPCR, quantitative polymerase chain reaction; SF, silk fibroin.

promote new bone formation more strongly than the pure PLCL scaffold in vivo.

Collectively, the SF/PLCL (50/50) nanofibrous scaffold supported the proliferation and osteogenic differentiation of hADSCs better than other scaffolds in vitro and promoted new bone formation more strongly than the pure PLCL scaffold in vivo.

Discussion

ADSCs are easily accessible and grow rapidly in vitro,[41,42] making them attractive seed cells for bone regeneration. In bone tissue engineering, it is rational to develop scaffolds with nanofibrous ultrastructure to chemically and structurally mimic the native ECM of bone. Several studies have revealed that the nanofibrous architecture of the scaffolds is beneficial to the proliferation and osteogenic differentiation of MSCs and osteoblasts.[12,43,44] PLCL has been chosen as a scaffold matrix in bone regeneration, mainly due to its excellent mechanical properties, good biocompatibility, and capacities of stimulating MSC osteogenic differentiation and new bone formation.[21–23,34] However, PLCL polymers have their own drawbacks in that the inertness, less-bioactive characteristics and hydrophobicity result in less-efficient biomaterial/cell interactions. The blending of two polymers is a simple method to retain both their characteristics and to compensate for the drawbacks of one component in a blend. Therefore, to overcome the disadvantages of PLCL and improve the properties of the PLCL scaffold, SF, a type of natural polymer with abundant functional groups that promote MSC osteogenesis and ECM mineralization,[29,30,45] was blended with PLCL to further fabricate hybrid scaffolds for bone tissue regeneration.

A suitable scaffold for bone tissue engineering should have appropriate surface roughness, wettability, and cell recognition sites, and these properties of the scaffold affect the adhesion and proliferation of the seed cells cultured on it.[46,47] In the present study, the blended scaffold of SF/PLCL (50/50) exhibited much better capacity for attachment and proliferation of hADSC than the PLCL scaffold. The possible reasons for this are as follows: a significant positive correlation between surface roughness and cell attachment as demonstrated in a previous study,[48] and the roughened surface facilitating cellular adhesion.[49] Our results showed that blending SF and PLCL increased the surface roughness and that the SF/PLCL (50/50) scaffold exhibited higher surface roughness than the pure PLCL scaffolds. Second, as to the wettability of the scaffold, the pure PLCL scaffold was hydrophobic, whereas the incorporation of SF dramatically

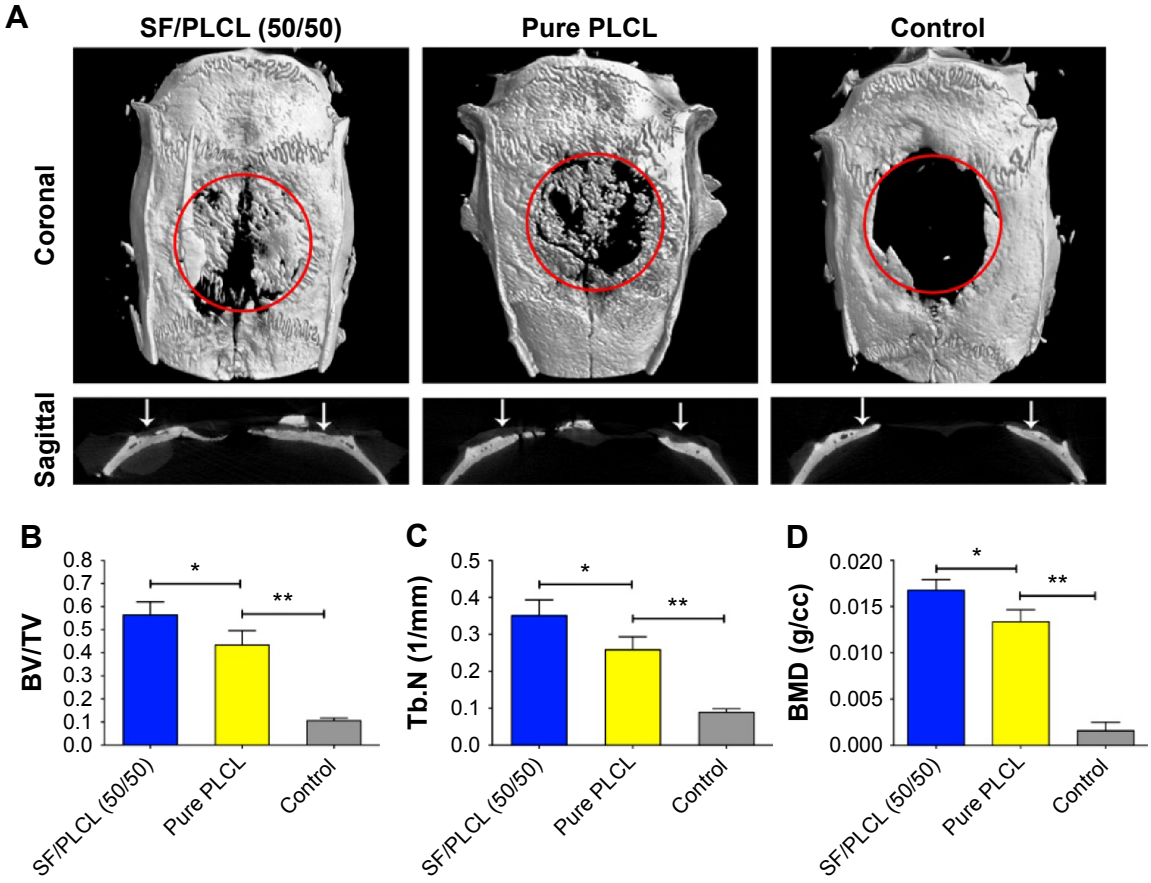

Figure 5 Microcomputed tomography imaging of the repaired skull after 12 weeks post-implantation.
Notes: (**A**) Representative 3D images and a sagittal view of harvested specimens showing the different reparative effects of hADSCs/SF/PLCL (50/50), hADSCs/pure PLCL, and the control groups. (**B**–**D**) BV/TV, Tb.N, and BMD variations in each group. *$P<0.05$, **$P<0.01$.
Abbreviations: BMD, bone mineral density; BV/TV, bone volume/total volume; hADSCs, human adipose-derived stem cells; PLCL, poly(lactide-co-ε-caprolactone); SF, silk fibroin; Tb.N, trabecular number.

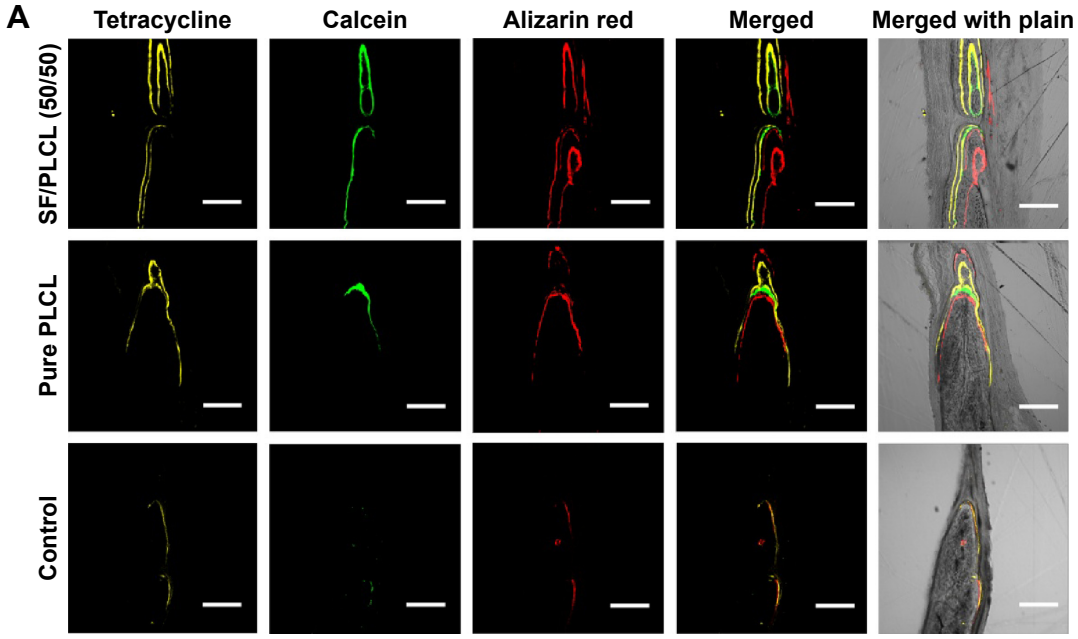

Figure 6 (*Continued*)

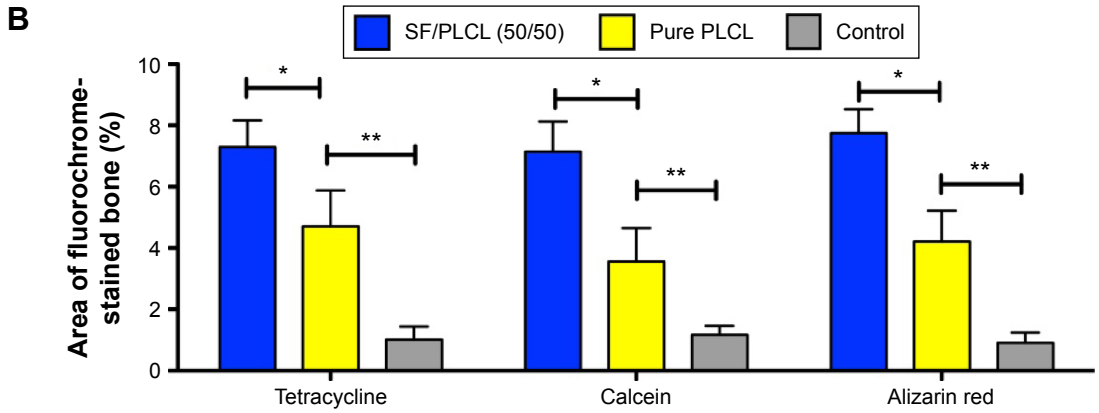

Figure 6 Fluorochrome labeling analysis of new bone formation and mineralization.
Notes: (**A**) Row 1 (yellow) shows tetracycline labeling at week 2; row 2 (green) shows calcein at week 4; row 3 (red) shows alizarin red at week 6; row 4 shows merged images of the three fluorochromes for the same group; and row 5 shows merged images of the three fluorochromes with the plain image for each group. (**B**) The percentages of each fluorochrome area for the different groups showed significant differences among the SF/PLCL (50/50), pure PLCL, and control groups. *$P<0.05$, **$P<0.01$.
Abbreviations: PLCL, poly(lactide-co-ε-caprolactone); SF, silk fibroin.

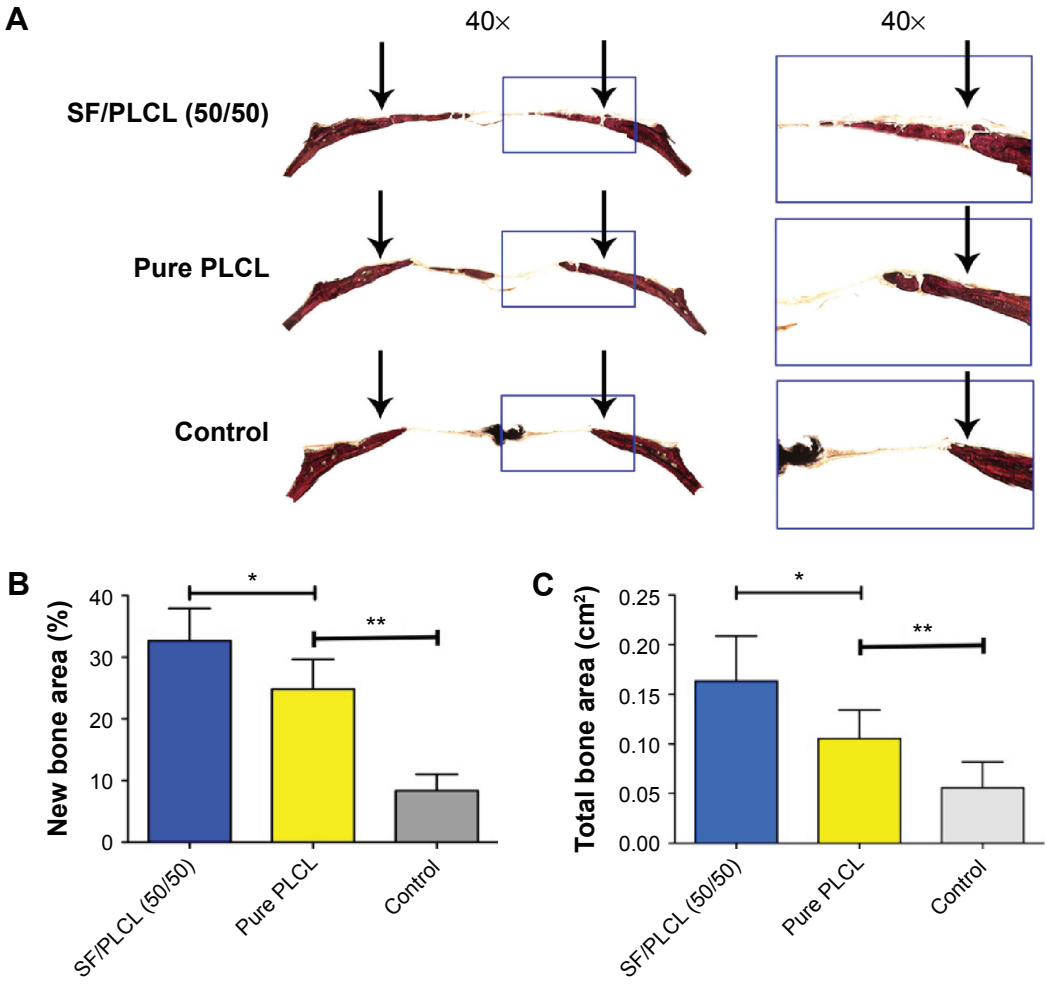

Figure 7 Histological evaluation of the newly formed bone.
Notes: (**A**) The sliced specimens were stained with van Gieson's picrofuchsin. Significant differences in reparative effects were observed among the SF/PLCL (50/50), pure PLCL, and control groups by analyzing (**B**) the newly formed bone area and (**C**) the percentage of newly formed bone with respect to total bone area. The arrows point out the fringe of the critical-sized calvarial bone defect. *$P<0.05$, **$P<0.01$.
Abbreviations: PLCL, poly(lactide-co-ε-caprolactone); SF, silk fibroin.

lowered the contact angle of the SF/PLCL nanofibrous scaffolds. The water contact angle of the SF/PLCL (50/50) scaffold was 62.02°±1.3°, which is in the range of favorable water contact angles (water contact angle 50°–70°) for cell attachment and proliferation.[50–52] Last but not least, the FTIR-ATR spectra and XRD curves of these scaffolds demonstrated that the blending of SF and PLCL did not change the characteristics of these two components and the blended SF/PLCL scaffolds possessed characteristics of both materials. Since synthetic polymers such as PLCL lack specific cell-recognizable signals for cell adhesion, functional groups such as $–NH_2$, –COOH, and –OH were incorporated onto the surface of nanofibers by adding SF to the blended scaffolds, thereby introducing more cell recognition sites for the adherence and proliferation of seed cells. Taken together, the combination of SF and PLCL was found to possess varying properties, and the SF/PLCL (50/50) scaffold exhibited the best performance in facilitating the adhesion and proliferation of hADSCs among these hybrid scaffolds, which may be due to the synergistic effects of appropriate surface roughness, suitable hydrophilicity, and the incorporation of functional groups on the surface of the scaffold.

The ideal scaffold for bone tissue engineering should not only facilitate the proliferation of seed cells but also enhance the osteogenic differentiation of seed cells, and the chemical–physical characteristics of the scaffold play important roles in regulating MSC osteogenic differentiation and ECM mineralization. First, it has been reported that rough surfaces enhance the ALP activity and extracellular calcium deposition of the osteoblast.[53] Our results showed that the SF/PLCL (50/50) scaffold (Ra=265 nm) had rougher surfaces than the pure PLCL scaffold (Ra=107 nm), and that the hADSCs cultured on the SF/PLCL (50/50) scaffold exhibited higher ALP activity and produced more mineralized ECM than the cells on the pure PLCL scaffold. Second, previous studies have revealed that SF could promote the osteogenic differentiation of MSCs by regulating the Notch signaling pathway;[45] additionally, SF could also facilitate ECM mineralization by regulating the formation of hydroxyapatite nanocrystals.[54–56] Our data showed that both the mRNA and protein levels of osteogenic-specific genes increased in hADSCs seeded on the pure SF, SF/PLCL (75/25), and SF/PLCL (50/50) scaffolds compared with the pure PLCL scaffold and that the SF/PLCL (50/50) scaffold exhibited the most significant elevation. SEM imaging showed large amounts of crystallized deposits attached to nanofibers on the surfaces of hADSCs seeded on scaffolds with higher SF weight ratios (pure SF, SF/PLCL [75/25], SF/PLCL [50/50]). Moreover, the results of ARS staining and semiquantitative assays showed similar patterns to those described earlier. Third, studies have shown that hydrophilic surfaces induce greater MSC osteogenesis and mineral deposition compared with hydrophobic surfaces.[57–59] In this study, the incorporation of SF improved the hydrophilicity of the scaffold, which may also have partially contributed to the enhanced osteogenic differentiation and ECM mineralization of the hADSCs seeded on the SF/PLCL (50/50) scaffold compared with the pure PLCL scaffold. Furthermore, the incorporation of SF into the PLCL scaffold also introduces abundant functional groups (–OH, –COOH, $–NH_2$) on the scaffold surface, which may also affect the osteogenic differentiation of MSCs and biomineralization of the ECM.[58,60,61] Hence, the elevated osteogenic markers and enriched mineralized ECM noted in this study may also be attributed to the involvement of functional groups. Above all, the SF/PLCL (50/50) scaffold exhibited the best osteoinductive property, which may be due to the synergistic influences of surface roughness, SF protein, hydrophilicity, and functional groups incorporated on the surface of the scaffold.

A CSD is the minimum defect that will not heal. As the SF/PLCL (50/50) scaffold exhibited better physical properties and cellular responses in all assessments in the in vitro study, we further investigated its effect on repairing CSD in rats, and the pure PLCL scaffold was used as a control based on its good performance in a previous work.[22] In the current study, a micro-CT analysis showed that the reparative effect of the composite of hADSCs and PLCL scaffold was significantly better than that of control (empty PLCL scaffold), which was consistent with a previous study reporting that MSC-seeded scaffold improves the healing of CSD.[40] Moreover, micro-CT analysis also revealed that the SF/PLCL (50/50) scaffold markedly promoted new bone formation compared with the pure PLCL scaffold. Histological analysis and fluorochrome labeling analysis further validated the finding that the SF/PLCL (50/50) scaffold performed better than the pure PLCL scaffold in repairing the CSD. Collectively, our data indicated that the SF/PLCL (50/50) scaffold meets the requirement for tensile strength in bone regeneration and enhanced in vivo new bone formation, compared with the pure PLCL scaffold.

Conclusion

Taken together, our data demonstrated that hADSCs cultured on SF/PLCL (50/50) scaffold exhibited high proliferation potential and strong osteogenic differentiation capacity in vitro. Moreover, SF/PLCL (50/50) scaffold seeded with hADSCs significantly enhanced new bone regeneration in

the repair of CSDs in rat, suggesting that electrospun SF/PLCL (50/50) nanofibrous scaffold holds great potential for bone tissue regeneration.

Acknowledgments

This work was supported by the National High Technology Research and Development Program (863 Program) (2015AA020311), National Natural Science Foundation of China (81320108010, 81170876, 31271029, 81570883), and the Shanghai Municipality Commission for Science and Technology (14JC1493103, 12419A9300). The authors express their sincere thanks to Dr Qiao from the Key Laboratory of Medical Molecular Virology, Ministry of Education and Public Health, Shanghai Medical School, Fudan University for technical assistance with confocal laser microscope imaging and Dr Zhang from Shanghai Key Laboratory of Orthopedic Implants, Shanghai Jiao Tong University School of Medicine for technical assistance with histological analysis.

Disclosure

The authors report no conflict of interest in this work.

References

1. Calori GM, Colombo M, Mazza EL, Mazzola S, Malagoli E, Mineo GV. Incidence of donor site morbidity following harvesting from iliac crest or RIA graft. *Injury*. 2014;45 Suppl 6:S116–S120.
2. Cui L, Liu B, Liu G, et al. Repair of cranial bone defects with adipose derived stem cells and coral scaffold in a canine model. *Biomaterials*. 2007;28:5477–5486.
3. Younger EM, Chapman MW. Morbidity at bone graft donor sites. *J Orthop Trauma*. 1989;3:192–195.
4. Gaines ST. Infection in bone allografts. Incidence, nature, and treatment. *J Bone Joint Surg Am*. 1988;70:1430–1431.
5. Huri PY, Ozilgen BA, Hutton DL, Grayson WL. Scaffold pore size modulates in vitro osteogenesis of human adipose-derived stem/stromal cells. *Biomed Mater*. 2014;9:045003.
6. Shi YY, Nacamuli RP, Salim A, Longaker MT. The osteogenic potential of adipose-derived mesenchymal cells is maintained with aging. *Plast Reconstr Surg*. 2005;116:1686–1696.
7. Mirsaidi A, Kleinhans KN, Rimann M, et al. Telomere length, telomerase activity and osteogenic differentiation are maintained in adipose-derived stromal cells from senile osteoporotic SAMP6 mice. *J Tissue Eng Regen Med*. 2012;6:378–390.
8. Egermann M, Heil P, Tami A, et al. Influence of defective bone marrow osteogenesis on fracture repair in an experimental model of senile osteoporosis. *J Orthop Res*. 2010;28:798–804.
9. Khan WS, Adesida AB, Tew SR, Andrew JG, Hardingham TE. The epitope characterisation and the osteogenic differentiation potential of human fat pad-derived stem cells is maintained with ageing in later life. *Injury*. 2009;40:150–157.
10. Rodriguez JP, Montecinos L, Rios S, Reyes P, Martínez J. Mesenchymal stem cells from osteoporotic patients produce a type I collagen-deficient extracellular matrix favoring adipogenic differentiation. *J Cell Biochem*. 2000;79:557–565.
11. Liang D, Hsiao BS, Chu B. Functional electrospun nanofibrous scaffolds for biomedical applications. *Adv Drug Deliv Rev*. 2007;59:1392–1412.
12. Li WJ, Tuli R, Huang X, Laquerriere P, Tuan RS. Multilineage differentiation of human mesenchymal stem cells in a three-dimensional nanofibrous scaffold. *Biomaterials*. 2005;26:5158–5166.
13. Ko EK, Jeong SI, Rim NG, Lee YM, Shin H, Lee BK. In vitro osteogenic differentiation of human mesenchymal stem cells and in vivo bone formation in composite nanofiber meshes. *Tissue Eng Part A*. 2008;14:2105–2119.
14. Rim NG, Lee JH, Jeong SI, Lee BK, Kim CH, Shin H. Modulation of osteogenic differentiation of human mesenchymal stem cells by poly[(L-lactide)-co-(epsilon-caprolactone)]/gelatin nanofibers. *Macromol Biosci*. 2009;9:795–804.
15. Lee JH, Rim NG, Jung HS, Shin H. Control of osteogenic differentiation and mineralization of human mesenchymal stem cells on composite nanofibers containing poly[lactic-co-(glycolic acid)] and hydroxyapatite. *Macromol Biosci*. 2010;10:173–182.
16. Yin Z, Chen X, Chen JL, et al. The regulation of tendon stem cell differentiation by the alignment of nanofibers. *Biomaterials*. 2010;31:2163–2175.
17. Rim NG, Kim SJ, Shin YM, et al. Mussel-inspired surface modification of poly(L-lactide) electrospun fibers for modulation of osteogenic differentiation of human mesenchymal stem cells. *Colloids Surf B Biointerfaces*. 2012;91:189–197.
18. Kwon IK, Kidoaki S, Matsuda T. Electrospun nano- to microfiber fabrics made of biodegradable copolyesters: structural characteristics, mechanical properties and cell adhesion potential. *Biomaterials*. 2005;26:3929–3939.
19. Jeong SI, Lee AY, Lee YM, Shin H. Electrospun gelatin/poly(L-lactide-co-epsilon-caprolactone) nanofibers for mechanically functional tissue-engineering scaffolds. *J Biomater Sci Polym Ed*. 2008;19:339–357.
20. Saik JE, McHale MK, West JL. Biofunctional materials for directing vascular development. *Curr Vasc Pharmacol*. 2012;10:331–341.
21. Chen L, Bai Y, Liao G, et al. Electrospun poly(L-lactide)/poly(epsilon-caprolactone) blend nanofibrous scaffold: characterization and biocompatibility with human adipose-derived stem cells. *PloS One*. 2013;8:e71265.
22. Kim JH, Kim MK, Park JH, Won JE, Kim TH, Kim HW. Performance of novel nanofibrous biopolymer membrane for guided bone regeneration within rat mandibular defect. *In vivo*. 2011;25:589–595.
23. Vergroesen PP, Kroeze RJ, Helder MN, Smit TH. The use of poly(L-lactide-co-caprolactone) as a scaffold for adipose stem cells in bone tissue engineering: application in a spinal fusion model. *Macromol Biosci*. 2011;11:722–730.
24. Kim BS, Mooney DJ. Development of biocompatible synthetic extracellular matrices for tissue engineering. *Trends Biotechnol*. 1998;16:224–230.
25. Chen J, Yan C, Zhu M, et al. Electrospun nanofibrous SF/P(LLA-CL) membrane: a potential substratum for endothelial keratoplasty. *Int J Nanomedicine*. 2015;10:3337–3350.
26. Zhang K, Wang H, Huang C, Su Y, Mo X, Ikada Y. Fabrication of silk fibroin blended P(LLA-CL) nanofibrous scaffolds for tissue engineering. *J Biomed Mater Res Part A*. 2010;93:984–993.
27. Wang Y, Rudym DD, Walsh A, et al. In vivo degradation of three-dimensional silk fibroin scaffolds. *Biomaterials*. 2008;29:3415–3428.
28. You R, Xu Y, Liu Y, Li X, Li M. Comparison of the in vitro and in vivo degradations of silk fibroin scaffolds from mulberry and nonmulberry silkworms. *Biomed Mater*. 2014;10:015003.
29. Jin HJ, Chen J, Karageorgiou V, Altman GH, Kaplan DL. Human bone marrow stromal cell responses on electrospun silk fibroin mats. *Biomaterials*. 2004;25:1039–1047.
30. Cai K, Yao K, Lin S, et al. Poly(D,L-lactic acid) surfaces modified by silk fibroin: effects on the culture of osteoblast in vitro. *Biomaterials*. 2002;23:1153–1160.
31. Prabhakaran MP, Venugopal J, Ramakrishna S. Electrospun nanostructured scaffolds for bone tissue engineering. *Acta Biomater*. 2009;5:2884–2893.
32. Correia C, Bhumiratana S, Yan LP, et al. Development of silk-based scaffolds for tissue engineering of bone from human adipose-derived stem cells. *Acta Biomater*. 2012;8:2483–2492.

33. Faghihi F, Baghaban Eslaminejad M, Nekookar A, Najar M, Salekdeh GH. The effect of purmorphamine and sirolimus on osteogenic differentiation of human bone marrow-derived mesenchymal stem cells. *Biomed Pharmacother*. 2013;67:31–38.
34. Jin GZ, Kim JJ, Park JH, et al. Biphasic nanofibrous constructs with seeded cell layers for osteochondral repair. *Tissue Eng Part C Methods*. 2014;20:895–904.
35. Xie Q, Wang Z, Bi X, et al. Effects of miR-31 on the osteogenesis of human mesenchymal stem cells. *Biochem Biophys Res Commun*. 2014; 446:98–104.
36. Deng Y, Bi X, Zhou H, et al. Repair of critical-sized bone defects with anti-miR-31-expressing bone marrow stromal stem cells and poly(glycerol sebacate) scaffolds. *Eur Cell Mater*. 2014;27:13–24; discussion 24–15.
37. Ni N, Zhang D, Xie Q, et al. Effects of let-7b and TLX on the proliferation and differentiation of retinal progenitor cells in vitro. *Sci Rep*. 2014;4:6671.
38. Zou D, Zhang Z, He J, et al. Repairing critical-sized calvarial defects with BMSCs modified by a constitutively active form of hypoxia-inducible factor-1alpha and a phosphate cement scaffold. *Biomaterials*. 2011;32:9707–9718.
39. Deng Y, Zhou H, Zou D, et al. The role of miR-31-modified adipose tissue-derived stem cells in repairing rat critical-sized calvarial defects. *Biomaterials*. 2013;34:6717–6728.
40. Xie Q, Wang Z, Huang Y, et al. Characterization of human ethmoid sinus mucosa derived mesenchymal stem cells (hESMSCs) and the application of hESMSCs cell sheets in bone regeneration. *Biomaterials*. 2015;66:67–82.
41. Wu PH, Chung HY, Wang JH, et al. Amniotic membrane and adipose-derived stem cell co-culture system enhances bone regeneration in a rat periodontal defect model. *J Formos Med Assoc*. Epub 2015 Jun 11.
42. Yoon E, Dhar S, Chun DE, Gharibjanian NA, Evans GR. In vivo osteogenic potential of human adipose-derived stem cells/poly lactide-co-glycolic acid constructs for bone regeneration in a rat critical-sized calvarial defect model. *Tissue Eng*. 2007;13:619–627.
43. Xin X, Hussain M, Mao JJ. Continuing differentiation of human mesenchymal stem cells and induced chondrogenic and osteogenic lineages in electrospun PLGA nanofiber scaffold. *Biomaterials*. 2007;28: 316–325.
44. Hu J, Liu X, Ma PX. Induction of osteoblast differentiation phenotype on poly(L-lactic acid) nanofibrous matrix. *Biomaterials*. 2008;29: 3815–3821.
45. Jung SR, Song NJ, Yang DK, et al. Silk proteins stimulate osteoblast differentiation by suppressing the Notch signaling pathway in mesenchymal stem cells. *Nutr Res*. 2013;33:162–170.
46. Curtis A, Wilkinson C. Topographical control of cells. *Biomaterials*. 1997;18:1573–1583.
47. Kim MS, Shin YN, Cho MH, et al. Adhesion behavior of human bone marrow stromal cells on differentially wettable polymer surfaces. *Tissue Eng*. 2007;13:2095–2103.
48. Deng Y, Liu X, Xu A, et al. Effect of surface roughness on osteogenesis in vitro and osseointegration in vivo of carbon fiber-reinforced polyetheretherketone-nanohydroxyapatite composite. *Int J Nanomedicine*. 2015;10:1425–1447.
49. Panda NN, Biswas A, Pramanik K, Jonnalagadda S. Enhanced osteogenic potential of human mesenchymal stem cells on electrospun nanofibrous scaffolds prepared from eri-tasar silk fibroin. *J Biomed Mater Res Part B Appl Biomater*. Epub 2014 Aug 30.
50. Grinnell F. Cellular adhesiveness and extracellular substrata. *Int Rev Cytol*. 1978;53:65–144.
51. Liu X, Lim JY, Donahue HJ, Dhurjati R, Mastro AM, Vogler EA. Influence of substratum surface chemistry/energy and topography on the human fetal osteoblastic cell line hFOB 1.19: Phenotypic and genotypic responses observed in vitro. *Biomaterials*. 2007;28:4535–4550.
52. Zhang D, Ni N, Chen J, et al. Electrospun SF/PLCL nanofibrous membrane: a potential scaffold for retinal progenitor cell proliferation and differentiation. *Sci Rep*. 2015;5:14326.
53. Wu Y, Zitelli JP, TenHuisen KS, Yu X, Libera MR. Differential response of Staphylococci and osteoblasts to varying titanium surface roughness. *Biomaterials*. 2011;32:951–960.
54. Takeuchi A, Ohtsuki C, Miyazaki T, Tanaka H, Yamazaki M, Tanihara M. Deposition of bone-like apatite on silk fiber in a solution that mimics extracellular fluid. *J Biomed Mater Res Part A*. 2003;65: 283–289.
55. Shanmugavel S, Reddy VJ, Ramakrishna S, Lakshmi B, Dev VG. Precipitation of hydroxyapatite on electrospun polycaprolactone/aloe vera/silk fibroin nanofibrous scaffolds for bone tissue engineering. *J Biomater Appl*. 2013;29:46–58.
56. Vetsch JR, Paulsen SJ, Muller R, Hofmann S. Effect of fetal bovine serum on mineralization in silk fibroin scaffolds. *Acta Biomater*. 2015;13: 277–285.
57. Park JH, Olivares-Navarrete R, Wasilewski CE, Boyan BD, Tannenbaum R, Schwartz Z. Use of polyelectrolyte thin films to modulate osteoblast response to microstructured titanium surfaces. *Biomaterials*. 2012;33:5267–5277.
58. Bodhak S, Bose S, Bandyopadhyay A. Role of surface charge and wettability on early stage mineralization and bone cell-materials interactions of polarized hydroxyapatite. *Acta Biomater*. 2009;5:2178–2188.
59. Eliaz N, Shmueli S, Shur I, Benayahu D, Aronov D, Rosenman G. The effect of surface treatment on the surface texture and contact angle of electrochemically deposited hydroxyapatite coating and on its interaction with bone-forming cells. *Acta Biomater*. 2009;5:3178–3191.
60. Curran JM, Fawcett S, Hamilton L, et al. The osteogenic response of mesenchymal stem cells to an injectable PLGA bone regeneration system. *Biomaterials*. 2013;34:9352–9364.
61. Curran JM, Chen R, Hunt JA. The guidance of human mesenchymal stem cell differentiation in vitro by controlled modifications to the cell substrate. *Biomaterials*. 2006;27:4783–4793.

Supplementary materials

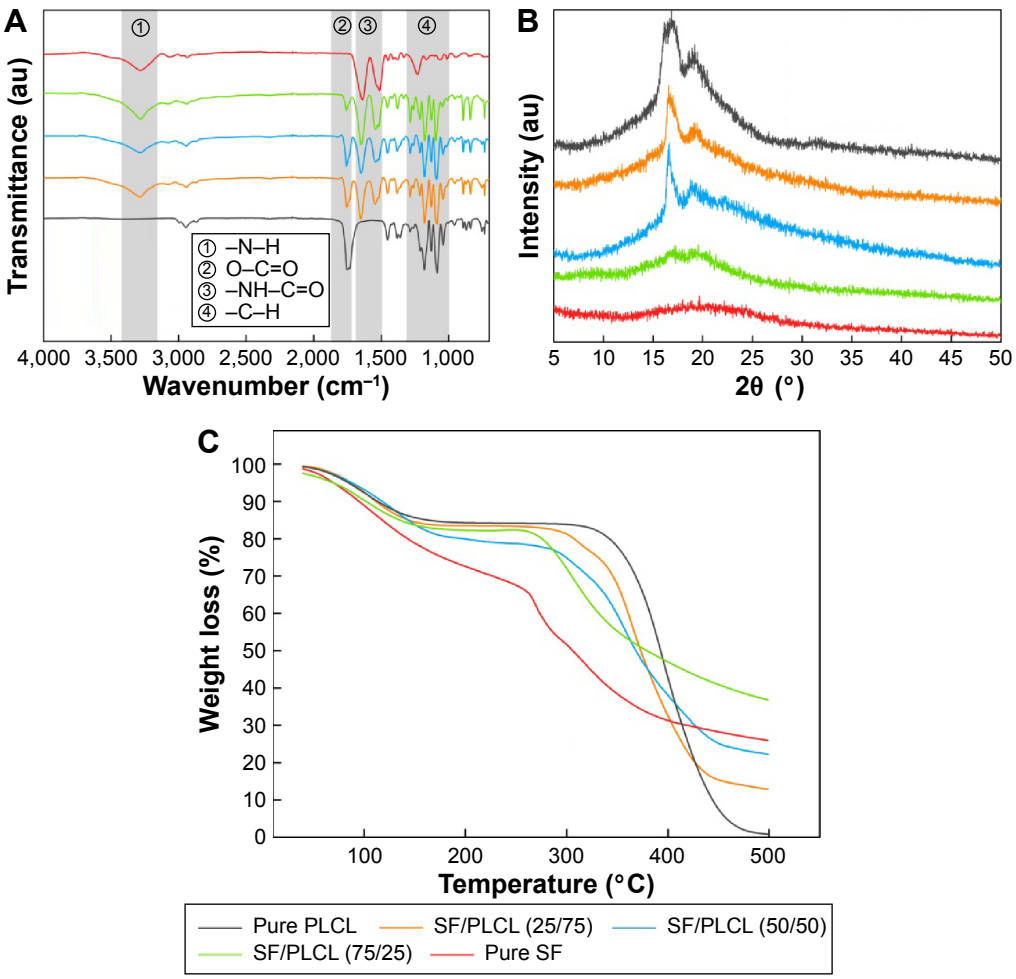

Figure S1 The phase structure and thermal analysis of SF/PLCL nanofibrous scaffolds of different weight ratios.
Notes: (**A**) FTIR-ATR spectra of SF/PLCL nanofibrous scaffolds of different weight ratios. (**B**) X-ray diffraction curves of SF/PLCL nanofibrous scaffolds of different weight ratios. (**C**) Thermogravimetric analysis curves of SF/PLCL nanofibrous scaffolds of different weight ratios.
Abbreviations: FTIR-ATR, Fourier transform infrared Attenuated total reflectance spectroscopy; PLCL, poly(lactide-co-ε-caprolactone); SF, silk fibroin.

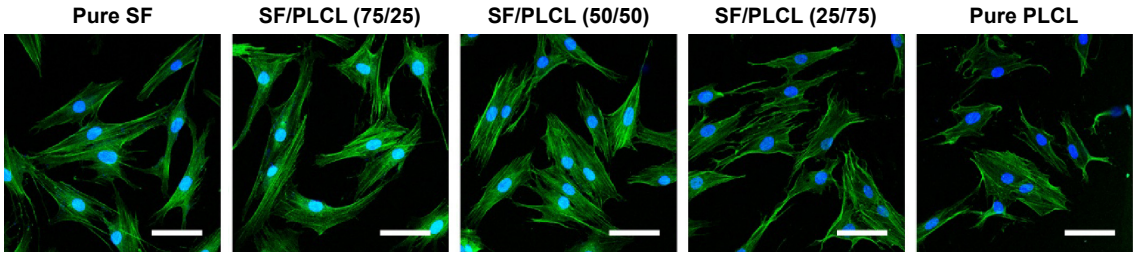

Figure S2 F-Actin of hADSCs seeded on SF/PLCL nanofibrous scaffolds of different weight ratios. Scale bars: 20 μm.
Abbreviations: hADSCs, human adipose-derived stem cells; PLCL, poly(lactide-co-ε-caprolactone); SF, silk fibroin.